Annals of Biomedical Engineering (2023) 51:2617–2628
https://doi.org/10.1007/s10439-023-03312-z

BMES BIOMEDICAL ENGINEERING SOCIETY

ORIGINAL ARTICLE

A Pneumatic Low-Pass Filter for High-Fidelity Cuff-Based Pulse Waveform Acquisition

Alessio Tamborini[1] · **Morteza Gharib**[1]

Received: 9 February 2023 / Accepted: 6 July 2023 / Published online: 21 July 2023

Abstract

Cuff-based pulse waveform acquisition (CBPWA) devices are reliable solutions for non-invasive cardiovascular diagnostics. However, poor signal resolution has limited clinical applications. This study aims to demonstrate the improved signal quality of CBPWA devices by implementing passive pneumatic low-pass filters (pLPF). Conventionally, pressure sensor output resolution is a percentage of the operating range. Therefore, measurement of small pressure changes in a large range must sacrifice signal resolution to accommodate for the large mean pressures. We design a pLPF to obtain the running mean pressure and combine it with a high-resolution differential pressure sensor for isolating the signal's pulsatile component. Thirty-one volunteers participated in a device proof-of-concept study at Caltech. Volunteers were measured at rest in the supine position on the left arm. The filtering behavior is mathematically modeled and experimentally verified, showing good agreement between measured and predicted cutoff frequencies. In the human study, the device successfully captured high-fidelity pulse waveform measurements for all volunteers: a blood pressure (BP) reading was followed by inflate-and-hold acquisition in diastolic BP (DBP), mean arterial pressure (MAP), and supra systolic BP (sBP). The study demonstrated the reliability and high signal resolution of pLPF for CBPWA. Considering the widespread use of the brachial cuff, a system for high-resolution CBPWA motivates the clinical implementation of non-invasive pulse waveform analysis (PWA).

Keywords Blood pressure measurement · Brachial cuff · Cardiovascular diagnostics · Pulse waveform analysis · *RC* filter

Abbreviations

BP	Blood pressure
CBPWA	Cuff-based pulse waveform acquisition
DBP	Diastolic blood pressure
IRB	Institutional Review Board
LPF	Low-pass filter
MAP	Mean arterial pressure
NIBP	Non-invasive blood pressure
pLPF	Pneumatic low-pass filter
PWA	Pulse waveform analysis
RC	Resistor-capacitor
SBP	Systolic blood pressure
sSBP	Supra systolic blood pressure

Associate Editor Arash Kheradvar oversaw the review of this article.

✉ Alessio Tamborini
atambori@caltech.edu

[1] California Institute of Technology, 1200 E California BLVD MC 105-50, Pasadena, CA 91125, USA

Introduction

Non-invasive PWA is a valuable diagnostic tool for assessing cardiovascular health. In the past, methodologies for PWA helped characterize cardiovascular features such as pulse wave velocity and augmentation index to inform therapeutic decisions better [1, 2]. The current clinical gold standard for non-invasive pulse waveform measurement is the tonometer, a handheld force sensor to measure arterial radial pulsations. Operation of tonometers on the peripheral artery requires arterial applanation: flattening of the arterial wall such that only internal pressure variations are measured. Overall, this process is time-intensive and needs a trained clinician. From a fluid dynamic perspective, the force applied at the artery compressing the walls influences local pressure-flow relationships. Inconsistency in this process impacts the repeatability of the results. For direct measurement of central pressure, a tonometer also requires the usage of the brachial cuff for BP calibration [3, 4]. These shortcomings severely limit the clinical application of PWA.

An alternative solution for capturing the pulse waveform is to utilize the brachial cuff with inflate and hold capabilities

[5–11]. The waveform is autonomously measured by maintaining the cuff at a constant pressure around the arm; the brachial artery radial pulsations will generate pressure fluctuations in the cuff proportional to the actual pulse waveforms. Controlling the cuff pressure ensures that the forcing condition is known and consistent throughout the measurement. The main shortcoming of CBPWA is low signal quality from pressure sensor tradeoffs between output signal resolution and operating range. CBPWA aims to capture a small pulsatile signal in a variable large mean pressure. Conventional implementation of a 12-bit pressure sensor to cover the entire measurement range (0–300 mmHg) limits output signal resolution to approximately 0.1 mmHg [10, 12]. Considering typical cuff signal amplitudes are on the order of one to three mmHg and pulse features are fractions of this amplitude, enhanced signal resolution is required for high-fidelity pulse waveform analysis [13]. To address this issue, it is optimal to focus the pressure sensor range only on the signal amplitude. One iteration of the traditional cuff device utilizes a solenoid air-valve and a differential pressure sensor to capture a base pressure as a measurement reference [14]. In this respect, the valve closure upon reaching the target-pressure would effectively create a constant pressure reservoir. A differential pressure sensor measures the difference between the signal and reservoir, effectively capturing the pulsatile component only. While this can capture small amplitude signals in an extended measurement range, practical implementation suffers significant data losses. Considering the system does not measure the mean pressure dynamically, any pressure decays that frequently occur in pneumatic systems must be corrected by active valve control. Such dynamic opening and closing of the solenoid air-valve result in pressure spikes and discontinuity within the recording [14].

In the approach presented in this paper, we propose a method to dynamically monitor mean pressure to isolate the pulse waveform using a passive pLPF and a single high-resolution differential pressure sensor. The pneumatic filter is modeled mathematically, and the model was used to optimize the filter for physiological conditions. The pLPF is incorporated in a cuff device for high-resolution pulse waveform acquisition and the device is enrolled in a proof-of-concept human study.

Materials and Methods

Sensor Principles

The cuff pressure signal has a static and a dynamic component. The static component originates from cuff inflation which, for human applications, ranges between 0 and 300 mmHg; this pressure reflects all physiological BP measurable with cuff systems. The dynamic component comes from pressure pulsations in the cuff which are on the order of two mmHg [13]. A differential pressure sensor outputs the pressure difference between the measurement and reference port. To accomplish our objective, the differential pressure sensor measures the difference between the full signal (static and dynamic components) and the signal mean (static part). The resulting output signal from the sensor is the dynamic component. The pLPF acts as a moving average filter and is connected to the reference port of the sensor to isolate the static component.

The pLPF is composed of a flow-limiting element and a compliant element in series (Fig. 1a). The flow-limiting element acts as a resistance in the pneumatic circuit, effectively reducing flow across it, this element will be referred to as *R*. The compliant element acts as a capacitance by storing the fluid from *R*, this element will be referred to as *C*. Together the *R* and *C* elements are designed to reduce and store airflow such that the output pressure will only be affected by sustained pressures. The combination of these elements creates the pneumatic *RC* filter.

Our high-fidelity pulse waveform acquisition device combines a passive pLPF with a differential pressure sensor to capture the small signal in an extended operating range (Fig. 2a). The sensor unit has two main components: the differential pressure sensor and the pneumatic *RC* filter. The differential pressure sensor is a Honeywell HSC Series differential pressure sensor with an operating range of ± 2 in H20 (± 3.73 mmHg), model number HSCDRRN002NDAA5. The sensor has a 0.03% full-scale span output resolution which translates to a 0.0022 mmHg resolution. The sensor's output is of the analog type with an update speed of 1 kHz; the sensor has an onboard analog-to-digital to-analog converter that limits update speed. The pneumatic *RC* filter comprises the *R* and *C* components (Fig. 1a). The *R* component is made from a rigid wall capillary tube with internal radius of 31.5 μm and length of 30 mm. The *C* component is made up of a rigid element and a compliant element. The compliant element is from an elastic line, and the rigid element is from rigid tubing and connectors with cylindrical internal volumes. The compliant tube is restricted in axial motion. The elastic tube has a length of 40 mm, internal radius of 0.8 mm, 0.8 mm wall thickness and 1.4 MPa elastic modulus. The rigid tube has a length of 36 mm and internal radius of 0.8 mm. The *RC* filter component properties are summarized in Table 1.

Mathematical Filter Modeling

Throughout this derivation, subscripts *R* and *C* refer to elements *R* and *C*, respectively. The mathematical model for the filter behavior assumes a conservation of mass between elements *R* and *C*, (1): all mass flowing through

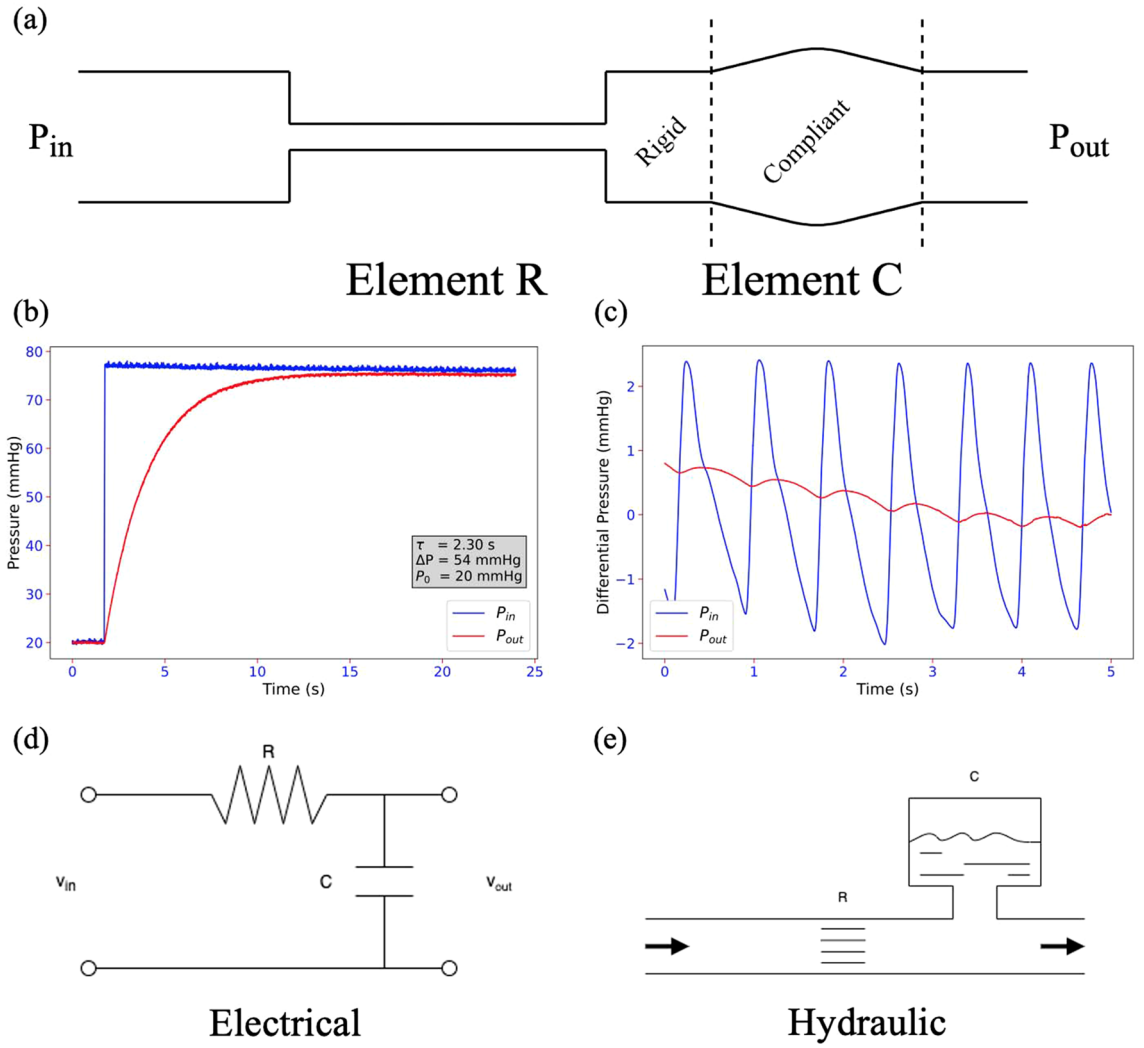

Fig. 1 **a** Schematic of the pneumatic filter including R and C elements. R element is the flow resistance. C element is the capacitive element with rigid and compliant parts; capacitance comes from tube compliance and gas compressibility. **b** Shows P_{in} and P_{out} for the step response of the system. Exponential decay curve fit parameters for P_{out} are summarized in text box. **c** Shows P_{in} and P_{out} from a differential pressure sensor for the filter exposed to pressure pulsations at the MAP hold. **d** An electrical equivalent system composed of a resistor and capacitor. **e** A hydraulic equivalent system composed of flow resistance and air capacitance chamber

R will affect the mass within the inner walls of C. Equation (1) is rewritten using the density and volumes as shown in (2). Both the density, ρ_c, and the volume of element C, V_c, are dependent on time and the equation can be expanded to give the form shown in (3). Considering the volume of element C is made up of both a compliant and rigid part, $V_c = V_{c_{\text{comp}}} + V_{c_{\text{rigid}}}$, the model has adjusted accordingly, as shown in (4).

$$\dot{m}_R = \frac{\mathrm{d}m_c}{\mathrm{d}t} \tag{1}$$

where $\dot{m}_R$ is the mass flow rate through element R, and $\frac{\mathrm{d}m_c}{\mathrm{d}t}$ is the rate of change of mass with time in element C.

$$\rho_R Q_R(t) = \frac{\mathrm{d}}{\mathrm{d}t}\left(\rho_c V_c\right) \tag{2}$$

where ρ_R and ρ_c are the fluid densities in elements R and C, respectively, $Q_R(t)$ is the volumetric flow rate through element R, and V_c is the volume of element C.

$$\rho_R Q_R(t) = \rho_c \frac{\mathrm{d}V_c}{\mathrm{d}t} + V_c \frac{\mathrm{d}\rho_c}{\mathrm{d}t} \tag{3}$$

$$\rho_R Q_R(t) = \rho_c \frac{\mathrm{d}V_{c_{\text{comp}}}}{\mathrm{d}t} + \left(V_{c_{\text{comp}}} + V_{c_{\text{rigid}}}\right)\frac{\mathrm{d}\rho_c}{\mathrm{d}t} \tag{4}$$

Table 1 Properties of the pneumatic low-pass filter

Element	Variable	Value
R	r_{R0}	31.5 µm
	L_{R0}	30 mm
$C_{\text{compliant}}$	r_{c0}	0.8 mm
	L_{c0}	40 mm
	h_{c0}	0.8 mm
	E_c	1.4 MPa
C_{rigid}	r_{c0}	0.8 mm
	L_{c0}	36 mm

where $V_{c_{\text{comp}}}$ is the compliant volume of element C and $V_{c_{\text{rigid}}}$ is the rigid volume of element C.

Element R only experiences pressure-driven flows. Flow in element R is characterized using Reynolds' Number (Re). An upper limit estimate solves to Re of 1084 by using Bernoulli's equation to calculate flow velocity from pressure gradient and a maximal pressure gradient of 300 mmHg along the element. As the maximum Re ~ 1000, all flows across element R fall in the laminar regime [15, 16]. Characterizing flow across R requires modeling two different scenarios. First, upon pump activation, the filter is exposed to a quasi-step function that persists till pressure equilibration. Considering the flow in R is fully developed (entrance length of 0.8 mm for a 30 mm tube), the pressure equilibration upon a step input can be instantaneously characterized using the Hagen Poiseuille flow solution. Secondly, the cardiovascular pulsatile pressure will dominate upon equilibration of input and output pressure. These flows are modeled with Womersley flows [17, 18]. Pulsatile flow in the system is described by a Womersley Number, α, of 0.04. For $\alpha < 2$, viscous forces dominate the flow developing a parabolic profile with in-phase pressure and velocity, this reduces the solution to real-components only [19, 20]. The lower limit of the Bessel function can be approximated as, $\lim_{x \to 0} J_0(x) = 1 - \frac{x^2}{4}$. Applying these

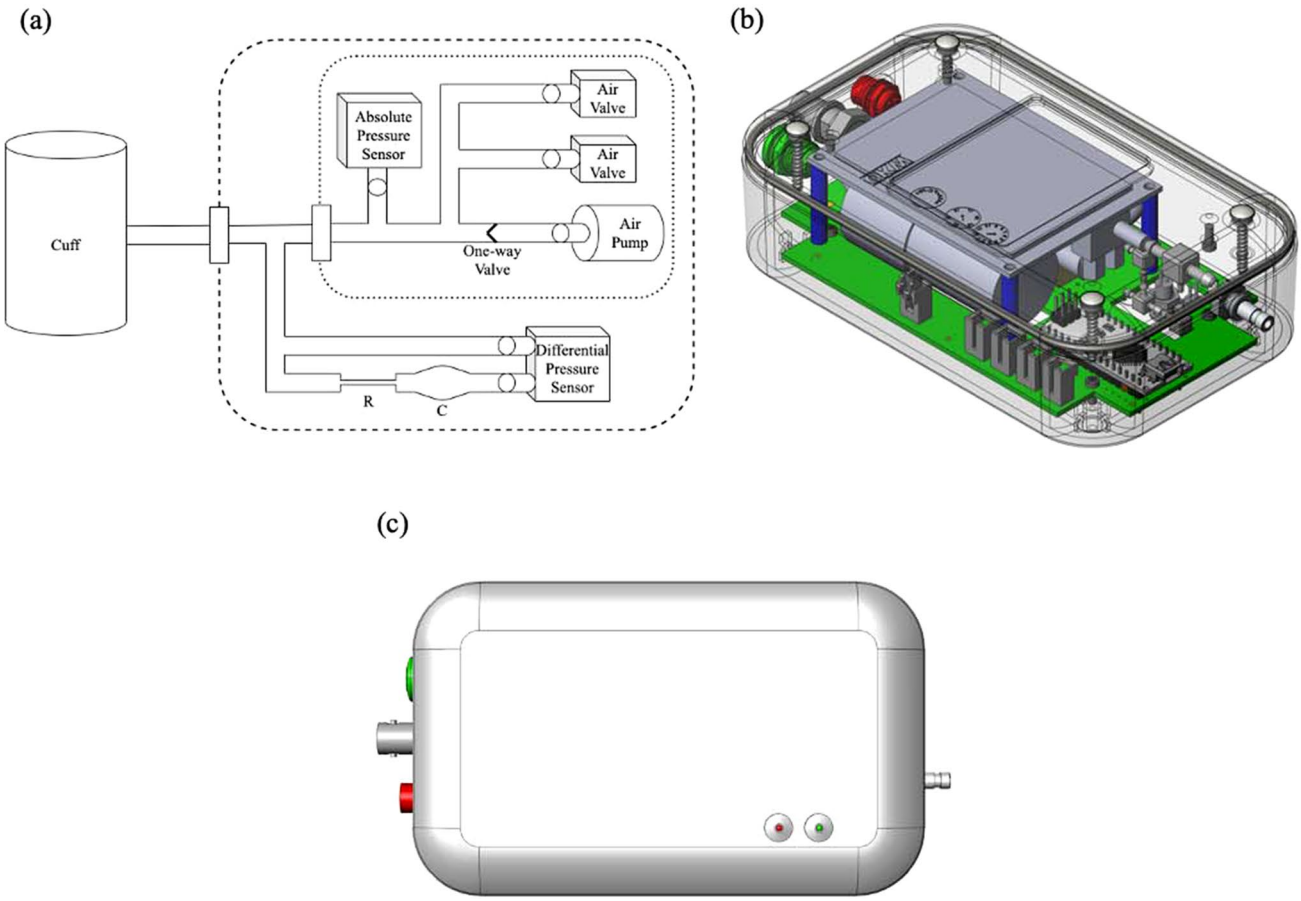

Fig. 2 A composition of the pulse waveform acquisition device from different perspectives. **a** shows the major pneumatic components of the device. Dashed line includes elements inside the device enclosure; the high-resolution acquisition system is composed of the R element, the C element, and the differential pressure sensor. Dotted line includes NIBP module components. Note components are not drawn to scale. **b** isometric view of device assembly rendering. Enclosure is shown transparent to highlight inside components. **c** device from top view emphasizing the casing and connection ports

simplifications to the Womersley flow equation and substituting the pressure gradient, P_n', with the pressure difference along the element's length, $-\Delta P_n/L$, gives (5). Solving for the volumetric flow rate gives (6), and substituting the pressure summation with a time dependent term (7) represents the pulsatile input pressure.

$$\lim_{\alpha\to 0} u(r,t) = \sum_{n=0}^{N} \frac{\Delta P_n}{4\mu L}\left(r_0^2 - r^2\right)\cos\left(n\omega t\right) \tag{5}$$

where u is the flow velocity, r is the radial coordinate, t is the time, α is the Womersley number, ω is the angular frequency of the first harmonic, n are the natural numbers, ΔP_n is the pressure gradient for the frequency $n\omega$, μ is the dynamic viscosity, L is the length of the tube, and r_0 is the internal radius.

$$Q(t) = \frac{\pi r_0^4}{8\,\mu L}\sum_{n=0}^{N}\Delta P_n\cos\left(n\omega t\right) \tag{6}$$

$$Q(t) = \frac{\pi r_0^4}{8\,\mu L}\Delta p(t);\;\; \Delta p(t) = \sum_{n=0}^{N}\Delta P_n\cos\left(n\omega t\right) \tag{7}$$

Pressure-to-radius models for elastic vessels characterize the behavior of flexible tubes undergoing pressure deformations [21, 22]. In the current design, the ratio of the internal radius to wall thickness has a value of 1. For thick-walled vessels $\left(r_0/h_0 < 10\right)$, the stress propagation in the vessel wall cannot be considered uniform and requires a more complex characterization of the stress profile. Taylor et al. solved the equation of motion for the pressure-to-radius relationship of a thick-walled elastic tube shown in (8) [23]. This relationship is converted to volume by accounting for the cylindrical structure of the compliant part of element C giving (9). Note that element C is axially constrained.

$$p_{tm} = K\left[\frac{r}{r_0} - 1\right];\; K = \frac{4}{3}\frac{Eh_0}{r_0}\theta_0;\; \theta_0 = \frac{1 + h_0/2r_0}{\left(1 + h_0/r_0\right)^2} \tag{8}$$

where p_{tm} is the transmural pressure, K is the tube's elasticity factor, r is the tube's internal radius, r_0 is the internal radius at zero transmural pressure, E is Young's modulus of the tube, h_0 is the tube wall thickness at zero transmural pressure, and θ_0 is the thickness factor.

$$V_{c_{\text{comp}}} = \pi r_0^2\left(\frac{p_{tm}}{K} + 1\right)^2 L \tag{9}$$

where V is the internal volume of the compliant tube and L is the axial length of the compliant tube.

The fluid in the system is air. Since the operating pressures and temperatures are close to the regular atmospheric regime, the behavior of air can be modeled using ideal gas laws with reasonable accuracy [24]. A relationship for the fluid's density is derived from the ideal gas law (10). Note that absolute tube pressure can be rewritten as $P_{\text{abs}} = P_{\text{atm}} + p_{tm}$ since the pressure outside the tube is atmospheric. P_{atm} is considered constant.

$$\rho = \frac{P_{\text{abs}}}{R_s T} \tag{10}$$

where ρ is the gas density, P_{abs} is the absolute pressure, R_s is the specific gas constant, and T is the gas temperature.

Equations (7), (9), and (10) are substituted in (3). The parameter λ is introduced to characterize the extension ratio for the elastic tube, $\lambda = r/r_0 = \left(p_{tm}/K_c + 1\right)$. Considering for most applications, this filter will be exposed to pressure fluctuations that are much smaller than the absolute pressure magnitude, $P_{\text{in}_{\text{abs}}} \approx P_{\text{out}_{\text{abs}}}$. Lastly, the undeformed volume of the compliant element in C will be expressed as $V_{c0_{\text{comp}}} = \pi r_{c0}^2 L_c$. These operations give the solution shown in (11).

$$\Delta p(t) = \frac{8\mu_R L_R}{\pi r_{R0}^4}\left(\frac{2V_{c0_{\text{comp}}}\lambda}{K_c} + \frac{V_{c0_{\text{comp}}}\lambda^2 + V_{c_{\text{rigid}}}}{P_{\text{in}_{\text{abs}}}}\right)\frac{\mathrm{d}p_{\text{out}_{tm}}}{\mathrm{d}t} \tag{11}$$

On the right-hand side of Eq. (11) is the time constant of the system in which the first term describes the viscous flow resistance, and the second term describes the capacitive effect composed of the tube compliance and the gas compliance, respectively. Substituting R for the viscous flow resistance and C for the capacitive term gives (12), a more common configuration for the RC filter equation.

$$\Delta p(t) = RC\frac{\mathrm{d}p_{\text{out}_{tm}}}{\mathrm{d}t} \tag{12}$$

where R is the resistance term, $R = \frac{8\mu_R L_R}{\pi r_{R0}^4}$, and C is the capacitance term, $C = \left(\frac{2V_{c0_{\text{comp}}}\lambda}{K_c} + \frac{V_{c0_{\text{comp}}}\lambda^2 + V_{c_{\text{rigid}}}}{P_{\text{in}_{\text{abs}}}}\right)$.

Device Components and Assembly

The device described herein is a cuff-based system with oscillometric algorithms for BP measurement and inflate and hold capabilities for non-invasive pulse waveform acquisition (Fig. 2). The electrical and pneumatic components of the device are contained within a medical-grade enclosure.

The electrical components perform the measurement sequence and are responsible to transmit the analog signal to the external data acquisition system. The main electrical components include the original equipment manufacturer non-invasive BP (NIBP) module, an Arduino nano, a differential pressure sensor, a digital-to-analog converter, and a relay. The Arduino Nano uses a ATMEGA328 chip with a

16 MHz clock speed. The device is powered using a medical grade 12 V power supply with a maximal current rating of 1.5 amps. The 12 V powers the NIBP module, the voltage is stepped down to 6 V to power the Arduino, and the 5 V output from the Arduino is used for the remaining components. Data out is in analog format from 0 to 5 V at an update speed of 1 kHz.

The pneumatic components are responsible for the pulse-sensing mechanism of the device. The main components include the BP brachial cuff, the connective tubing, the *RC* filter, and the quick connector for the cuff. The device uses tubing with an elasticity of 24 MPa, 1.59 mm internal radius, and 1.59 mm wall thickness for external connections. For internal connections, the device uses tubing with an elasticity of 24 MPa, 0.79 mm internal radius, and 0.79 mm wall thickness.

The NIBP module is a programmable BP measuring unit with tourniquet capabilities from PAR Medizintechnik. The BP measurement is performed using the oscillometric method in inflation (default) or deflation mode. The tourniquet mode allows the user to define a target pressure and hold time. Bidirectional connection with the board is performed via serial asynchronous communication with a baud rate of 4800 Baud. The device uses an Arduino Nano as the central micro-controller that controls and performs the measurement sequence. The original equipment manufacturer NIBP module is certified by the manufacturer, PAR Medizintechnik, to meet basic electrical safety according to the standard EN 60601-1 and for safety requirements of the BP measurement IEC 80601-2-30.

Device Measurement

The measurement has two stages: (1) BP measurement and (2) pressure hold. The BP measurement is a regular oscillometric BP measurement; the system default is inflation mode yet reverses deflation automatically upon failure. The output of the BP measurement is the SBP, DBP, MAP, and heart rate. Result communication occurs via the analog output. The pressure holds were performed using an inflate and hold methodology on subject-specific pressures; the measurement performs three holds at DBP, MAP, and sSBP (SBP + 35 mmHg) for 30, 20, and 40 s, respectively. Each hold will initiate a communication of the target pressure. During the hold, the signal from the differential pressure sensor is directly outputted from the device at an update speed of 1 kHz. Simultaneously, the nominal cuff pressure at integer precision is stored. Upon termination of the hold time, the nominal cuff pressure is then outputted to the DAQ.

Pulse Waveform Calibration

The pulse waveform measured with the device is in units of mmHg (or V) reflective of the pressure pulsations in the brachial cuff (Fig. 5). To generate a physiologically significant analytical tool, the waveform must be calibrated with BP values. The calibration process involves converting the raw voltage (or mmHg) waveform to the physiological BP scaling [25, 26]. Individual pulsations from a pressure hold are identified using the pulse indices. Iteratively, each pulsation is min–max scaled from 0 to 1, multiplied by the pulse pressure (SBP-DBP), and added to the base of DBP. The process will convert all pulsations to physiological BP units. For visualization purposes, the pulsations can be mathematically concatenated. To account for pressure fluctuations related to breathing, the average signal movement during the hold is used to scale each pulsation. The scaling factor is constant between individuals to have a uniform methodology.

Filter Step Response Tests

The characteristics of the *RC* filter were evaluated with an experimental setup to measure the model's step response. The setup measures the input and output pressure across the *RC* filter. A large reservoir is used as the pressure source and is pressurized using a hand pump. The large reservoir is connected to the filter with an on-off air valve. The pressure-based step response was generated by opening the on-off

Table 2 Case report form characteristics summary of the IRB study population

Variable	Quantity ($n = 31$)
Age, mean (years)	29 ± 10
Men, *n* (%)	21 (67)
Weight, mean (kg)	73 ± 11
Height, mean (m)	1.75 ± 0.09
BSA, mean (m^2)	1.89 ± 0.19
BMI, mean (kg/m^2)	23.8 ± 3.0
Left arm circumference, mean (cm)	29 ± 5
White, *n* (%)	25 (81)
Hypertension, *n* (%)	1 (3)
Diabetes, *n* (%)	1 (3)
Thyroid, *n* (%)	1 (3)
Hyperlipidemia, *n* (%)	4 (12)
Smoker, *n* (%)	8 (26)
Blood pressure medication, *n* (%)	2 (6)
Cardiovascular diseases, *n* (%)	0 (0)

valve between the reservoir and filter while a pressure delta was present across the valve. The experiment provided a fifty mmHg pressure step. Starting pressures, defined as the transmural pressure in the filter at start time, between 0 and 250 mmHg, were evaluated at 25 mmHg intervals. The tests were repeated three times for each starting pressure. The experimental cutoff frequency was estimated by extracting the time constant from an exponential decay curve fit to the step response output pressure and converting to frequency using the following equation, $f_0 = (2\pi\tau)^{-1}$.

Physiological Data Acquisition

Institutional Review Board (IRB) approval was obtained at Caltech for a device functionality and proof-of-concept study (Protocol number 21-1114; approval date on September 17th, 2021). The device collected physiological data from healthy volunteers ($n = 31$) at Caltech from May 17th, 2022, to June 2nd, 2022. Informed consent was obtained from all volunteers before testing by the physician (F.P.). All methods were carried out in accordance with relevant guidelines and regulations. Work adheres to the Declaration of Helsinki. Exclusion criteria included obstructions on the left arm impeding the BP cuff and any reported cardiovascular events. All volunteers were tested on the left arm in the supine position after a 5-min rest period. Patient characteristics, medical history, and cardiovascular influencing factors were all recorded as part of a health assessment questionnaire prior to testing; this form was completed with the self-reported data from study participants. Data were de-identified upon collection to protect subject privacy. Study population information has been summarized in Table 2; 21 volunteers were men and had an average age of 30 ± 11 years old and 10 volunteers were female and had an average age of 28 ± 8 years old.

Results

Mathematical Characterization of pLPF

The cutoff frequency for the pLPF can be evaluated using numerical methods on the R and C constants with the reference values from Table 1. The R constant is dependent on the viscous flow resistance generated within the R element. The C constant is dependent on both the gas compressibility and the tube compliance within the C element. To ensure the validity of this approach, the R and C constant units were assessed. The R term, $\frac{8\mu_R L_R}{\pi r_{R0}^4}$, has units of $\frac{kg}{m^4 s}$. The C term, $\left(\frac{2V_{c0_{\text{comp}}}\lambda}{K_c} + \frac{V_{c0_{\text{comp}}}\lambda^2 + V_{c_{\text{rigid}}}}{P_{\text{in}_{\text{abs}}}}\right)$, has units of $\frac{m^4 s^2}{kg}$. Combining the R and C terms gives units of seconds that match the expectations for a time constant. The relationship to calculate cutoff frequency from the time constant is given by $f_0 = (2\pi\tau)^{-1}$, where τ is given by the R and C constants. The filter's calculated cutoff frequency has a dependence on the system's input pressure as observed in the C term. The pressure dependence of the cutoff frequency originates from the tube

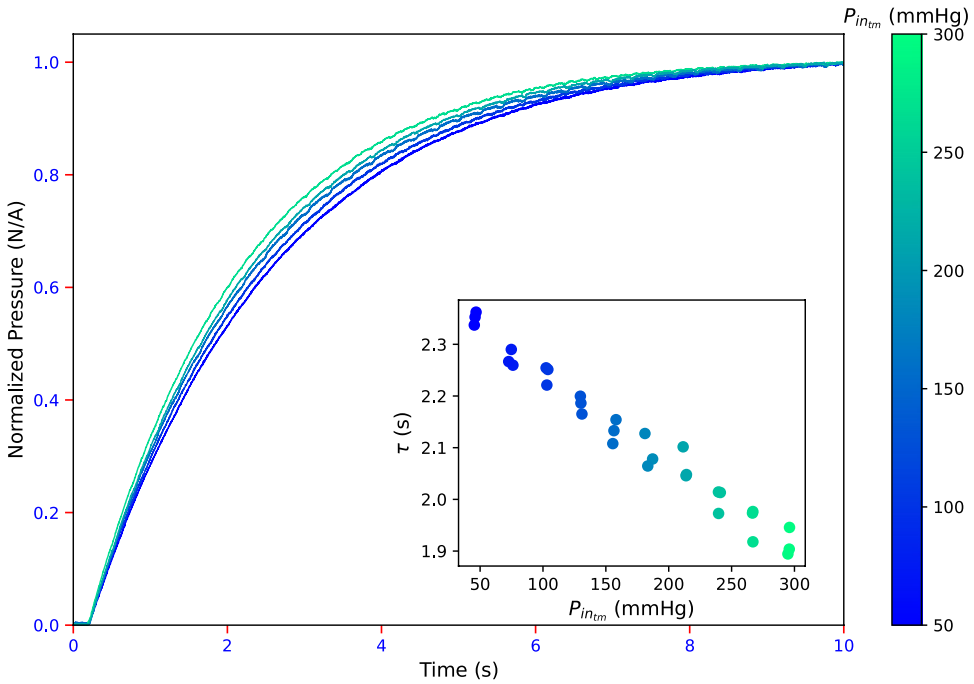

Fig. 3 Normalized transmural output pressure, $P_{\text{out}_{tm}}$, as a function of time for the pneumatic filter subject to a step pressure input. For clarity, only a subset of the trials is shown. The color bar indicates the transmural input pressure. The inset shows the optimized step response time constant as a function of $P_{\text{in}_{tm}}$, all trials are shown

compliance in the λ term and the change in gas compressibility from the $P_{\text{in}_{\text{abs}}}$ term.

Equation (8) gives an estimated maximal strain in the compliant element of 0.057 for a transmural pressure of 300 mmHg. The minimal tube strain suggests the system can be approximated with good precision with $\lambda = 1$. Simplifying the system with the $\lambda = 1$ approximation, gives a pressure dependent linear error with the actual model when calculating cutoff frequency; maximal error of 6.5% occurs at 300 mmHg. Numerical evaluation of the capacitive effect contributions results in 86.8% from gas compliance and 13.2% from tube expansion, indicating that the dominant effect originates from gas compressibility.

Step Response of pLPF

In response to a pressure step input, the pneumatic filter always generated exponential shape outputs typical of a low-pass filter (LPF); an example is shown in Fig. 1b. For each experimental trial, the exponential decay equation was curve fit to solve for the system's time constant. The experimental results in Fig. 3 confirm the pressure dependence of the system's time constant. The exponential time constant can be observed to decrease from 2.36 to 1.89 s as we increase the pressure from 50 to 300 mmHg (see inset of Fig. 3).

Validation of pLPF Characteristics

The estimated cutoff frequency from the mathematical model and the experimental step response tests showed a high degree of correspondence within the range of 0.0675 to 0.0825 Hz (Fig. 4). In both cases, a positive dependence between pressure and cutoff frequency was observed. The relationship between the cutoff frequency and the transmural pressure in the experimental model can be approximated with a linear regression (slope = 6.05×10^{-5} Hz/mmHg and intercept = 0.065 Hz). This model helps estimate the cutoff frequency at a given operating pressure. The experimental data measures an increase of 0.017 Hz in the cutoff frequency within the tested pressure ranges using the linear model presented above. Similarly, the theoretical results report a rise of 0.013 Hz.

Dynamic Response of pLPF

Dynamic filter behavior was qualitatively analyzed on a physiological pulsatile signal from a MAP hold. The cuff was inflated to the MAP pressure, and the input and output pressures were measured. An example of the filter behavior to a pulsating signal is shown in Fig. 1c. The input pressure (blue) is the pulsating signal, and the filtered output pressure (red) is the pLPF signal output. The measured output signal has a significantly reduced amplitude consistent with the expected behavior of an LPF.

Device Measurement on Human Subjects

The device successfully captured the pulse waveform in high resolution on 31 subjects during the IRB study. The study enrolled a healthy control group within the Caltech population. The data collected in the health assessment questionnaire for each study volunteer is summarized is Table 2. The minimal prevalence of comorbidities

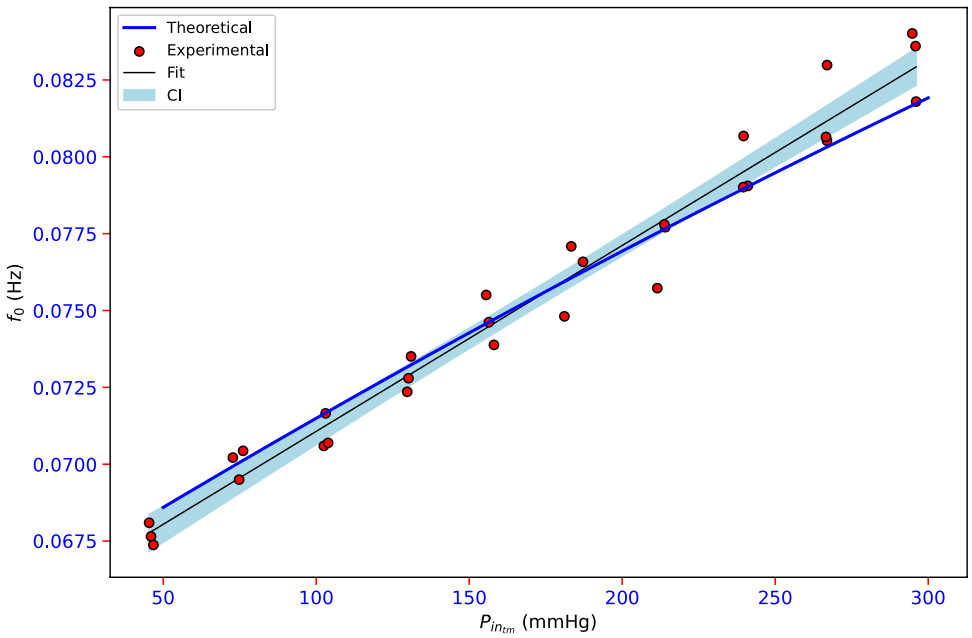

Fig. 4 Filter's cutoff frequency as a function of the transmural input pressure $P_{\text{in}_{tm}}$. Cutoff frequency from the mathematical model is shown as a solid line (blue). The scatter plot (red) shows data from the step response experiment with a linear regression (black) and confidence intervals (light blue) overlayed

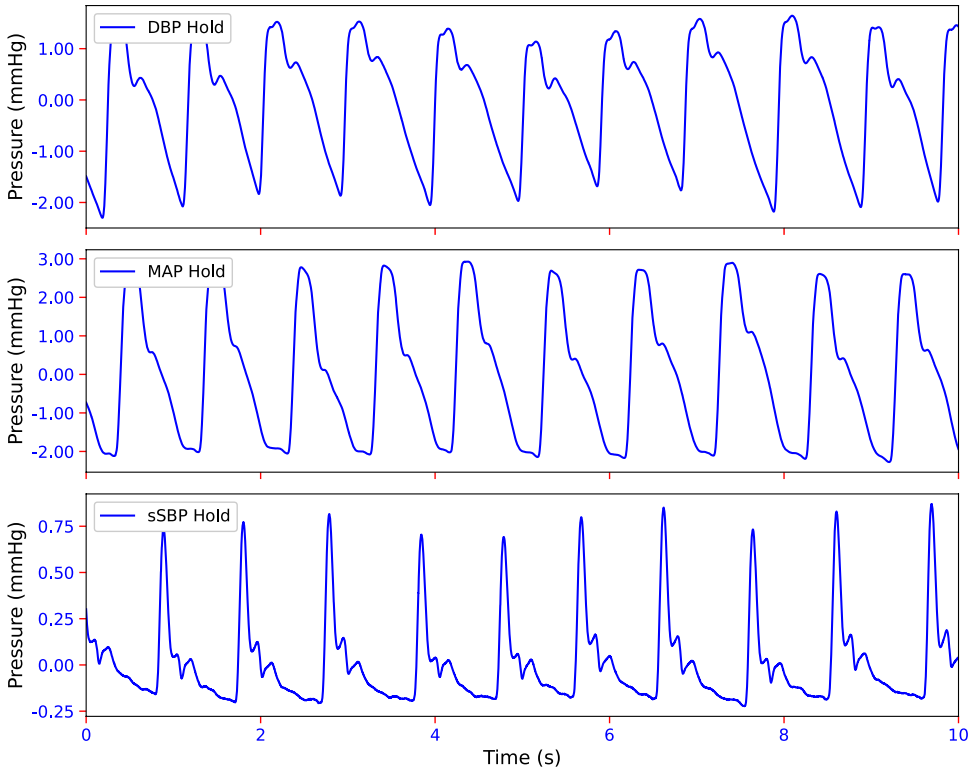

Fig. 5 Uncalibrated high-resolution pulse waveform signals as measured with the differential pressure sensor in a study participant. Pressure hold values were selected from the subjet-specific BP measurement. (Top) shows the DBP hold pressure pulse waveform signal. (Middle) shows the MAP hold pressure waveform signal. (Bottom) shows the sSBP hold pressure waveform signal. Note: signals are sequentially captured during the measurement and are not simultaneous

confirms the good health of the selected population. For each subject, the procedure consisted of a complete device measurement: the BP measurement followed by the DBP, MAP, and sSBP pressure holds. Of the 31 BP measurements, 27 (87%) were performed in the default inflation mode, and 4 (13%) automatically resorted to deflation mode. Case-specific reasons for switching to deflation mode are unknown but usually fall within one of the following conditions: low signal amplitude, noisy measurement, or irregular heart rhythm. In all 31 measurements, the BP holds were performed sequentially following the BP measurement with the subject-specific values. The DBP, MAP, and sSBP hold had an inflation time of 30, 20, and 40 s, respectively. The pressure hold waveforms displayed features used in PWA. Furthermore, as shown in Fig. 5, the waveforms display physiological pressure fluctuations from breathing. Examples of the calibrated and segmented waveforms from four individuals for all pressure holds have been depicted in Fig. 6. The device was successfully operated using the remote controller, and all the operator communications were directly interpretable from the DAQ without the need to access the device.

Discussion

The mathematical model for the pneumatic *RC* filter presented herein fully characterizes the behavior observed during experimentation, as shown in Fig. 4. The pLPF is composed of two separate elements that contribute to the observed behavior: the resistive and capacitive elements. The resistive element, in the form of a narrow tube, offers high resistance to flow, effectively creating laminar flows with predominant viscous characteristics. On the other hand, the capacitive element in this configuration is formed by the combination of the compliant tube and the compressibility of the fluid: both elements store mass in the form of pressure. The linear pressure-radius relationship describes the compliant tube characteristics, and this element expands to accommodate a larger mass as the pressure increases. The compressibility of the fluid is characterized by the increase in fluid density with pressure; as pressure increases, the fluid stores a larger quantity per unit volume. The series combination of the R and C elements displays the characteristics of an LPF in the fluid dynamic domain.

The pLPF characteristic R and C terms are numerically evaluated to measure the system's time constant, τ, as a function of pressure and calculate the cutoff frequency.

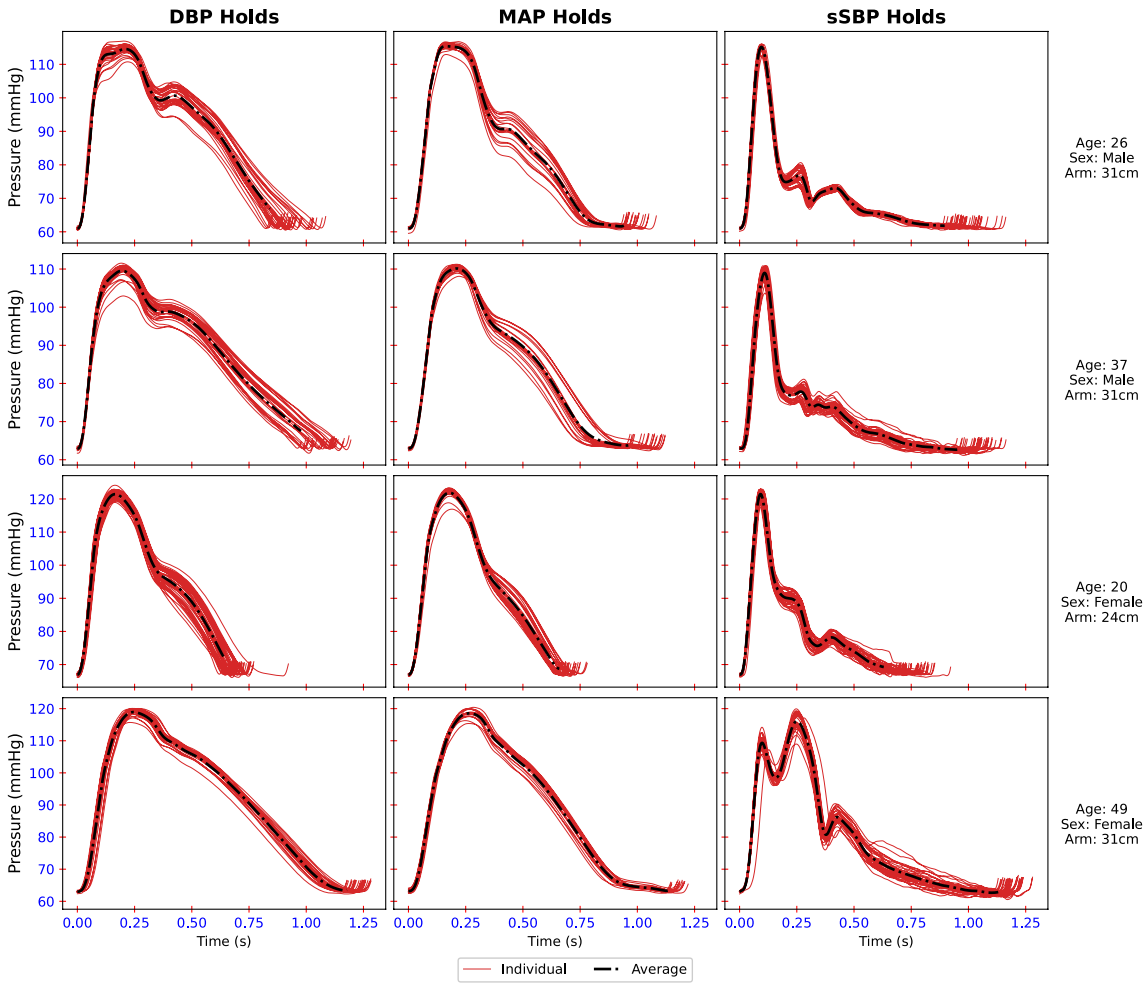

Fig. 6 Shows the calibrated and segmented pulse pressure waveforms for four volunteers in the IRB study. Rows separate study participants and columns separate holds: first column is DBP hold, second column is MAP hold, and third column is sSBP hold. Subject characteristics are displayed on the right side

The device's geometrical and structural property configuration gives a theoretical cutoff frequency between 0.069 and 0.082 Hz. These values were experimentally validated with the cutoff frequency extracted in the step response experiment. The experimental cutoff frequency was estimated by extracting the time constant from the exponential decay curve fit to the step response output pressure and converting to frequency. As shown in Fig. 4, the magnitude of the system's calculated and measured cutoff frequencies establish good accordance. In the current system configuration, the capacitive element in the pLPF has been shown to predominantly originate from the gas compressibility effect. The tube strain and consequently tube compliance effect are minimal throughout the operating range of the device. These findings would allow to simplify the model by order reduction while maintaining good precision. The scope of a pLPF goes beyond pulse waveform acquisition, and the mathematical model proposed herein can be used to design the filter for additional applications.

In this study, we formulated and experimentally validated the design of a pLPF constructed by a resistive element and a capacitive element. The construction of this filter in the pneumatic domain closely matches the composition of an *RC* LPF in the electrical domain: a resistor connected in series with a capacitor (Fig. 1d). Both pneumatic and electrical LPF are first order systems and as such have similar exponentially decaying step responses. Electronic-hydraulic analogies are conventionally used to enhance the understanding of electronic systems by comparison with hydraulic components and vice versa. The electrical *RC* LPF can be understood as the time required to charge/discharge the capacitor through the resistor. Similarly, the pLPF can be described as the time required to accumulate/empty mass through the flow resistive element. Furthermore, the *R* and *C* terms in the pneumatic filter equation were shown to have

the same equivalent units to the electrical resistance and capacitance. Ultimately, these results expand the knowledge of pneumatic components within a fluid dynamic realm and give the mathematical tools to characterize the response.

In the context of non-invasive pulse waveform acquisition devices, a cuff-based system addresses multiple of the tonometer's limitations. Yet, due to the low resolution of the captured pulse waveform, these systems have not been adopted in the cardiovascular field. Pressure sensors face a tradeoff between operating pressure range and output signal resolution. For pulse waveform acquisition with cuff devices, the required operating range is significantly larger than the signal amplitude posing a bandwidth challenge in the measurement. As such, implementation of a software-based filtering approach on the cuff pressure signal does not address the source of the limitation that lies in the output signal resolution. One previous attempt to address this issue used a solenoid air valve to generate a static mean signal as a measurement reference on the differential pressure sensor. Yet this approach suffered severe data losses and pressure spikes from valve operation [14]. This paper proposes a new high-fidelity pulse waveform acquisition approach by combining a passive pLPF and a high-resolution differential pressure sensor. The differential pressure sensor measures the difference between the mean and pulsatile signals in the measurement port and the mean of the signal in the reference port. The pLPF acts as a moving average filter allowing the differential pressure sensor to operate at a net differential pressure of zero. With the pLPF, the differential pressure sensor range can now target the signal amplitude rather than the full BP regime resulting in a significant increase in output signal resolution. In such a way, the pressure sensor always operates around a zero differential regardless of the pressure behavior and the enhanced signal resolution fully resolves pulse waveform features. Considering cuff-based pulse signals' well-defined bounds and characteristics, a single filter conformation is designed to fit all BP physiological operating ranges. The structure of this pneumatic filter requires minimal hardware components to configure an NIBP module with tourniquet capabilities for high-resolution pulse waveform acquisition: the pLPF and the differential pressure sensor. Overall, this configuration proves to be a good solution for high-resolution CBPWA.

The device was enrolled in a proof-of-concept study at Caltech under IRB Protocol number 21-1114 to validate the concept of a passive pLPF for high-resolution pulse waveform acquisition. The device successfully captured the pulse waveform in all three pressure holds throughout the study. The morphology of the pulse pressure waveform showed consistent behavior in all volunteers: the MAP waveforms are the largest in amplitude, and the sSBP is the waveform with the most critical pressure information. This result indicates that the device successfully uses the BP measurement to perform holds at subject-specific targets. The pressure hold recordings also displayed the dynamic behavior of the cardiovascular system in response to breathing. In Fig. 5, we can qualitatively observe how all three have the signal amplitude and mean fluctuation in response to breathing. Furthermore, the sSBP hold signal also shows waveform morphology variations from breathing, consistent with behaviors observed in invasive catheter measurements [27]. Within the limited ranges tested in this study, physical characteristics, including age, gender, height, weight, and left arm circumference, did not affect the recording quality.

A cuff-based system allows accurate control of the forcing condition on the brachial artery during measurement. Arteries behave such as collapsible elastic vessels when exposed to cuff pressure; the internal radius collapses upon external pressure exceeding internal pressure. From a fluid-solid interaction perspective, multiple holds interrogate the cardiovascular system at different flow conditions. This device configuration captures data at the DBP, MAP, and sSBP hold, corresponding to full, partial and no flow conditions. As shown in Fig. 6, the features present in the pulsations vary with the hold pressure, which indicates how flow and pressure interact.

Although the findings in the study aim to improve the methods for cuff-based non-invasive pulse waveform acquisition, there are several limitations that must be discussed. The population of this study focused on young and healthy individuals. With aging and the onset of disease, multiple cardiovascular and physical factors influence the strength and quality of the pulse waveform throughout the body. This will inevitably affect the quality of the non-invasive recording at the brachial artery [28]. Further testing of the device on a more diverse population will be necessary to fully optimize the system's configuration. Also, the mathematical characterization of the pLPF has only verified the filter behavior within the device's operating range in the time domain. Typically, filters are best characterized in the frequency domain with the Bode magnitude and Bode phase plots. A more in-depth mathematical analysis must evaluate the pLPF model in the frequency domain for full characterization.

With the rise of cardiovascular disease in the U.S. and worldwide, improving non-invasive pulse waveform acquisition methodologies for diagnosis and patient monitoring is essential. This study demonstrated the feasibility of using passive pneumatic filters to obtain high-resolution pulse waveform data with cuff-based devices. This is achieved using pLPFs on the reference port of the high-resolution differential pressure sensors to capture the mean pressure as a measurement base dynamically. The study also presents a mathematical model that characterizes the pLPF, optimizing the filter for various physiological

conditions. The improved signal quality from the proposed approach for cuff-based BP devices allows for a more widespread application of non-invasive pulse waveform acquisition both in the clinic and at home.

Acknowledgments The authors of this paper would like to acknowledge David Jeon for the technical support, Prof. John E. Sader for the scientific discussions, and Dr. Francisco Padilla for the data collection during the IRB study.

Funding This work was supported in part by the Cherng Fellowship from the Andrew and Peggy Cherng Department of Medical Engineering at Caltech and in part by the Gakenheimer Fellowship.

Declarations

Conflict of interest A. Tamborini and M. Gharib have a pending patent with the USPTO and PCT for the system described. Caltech is in negotiation for potentially licensing the patent to a biomedical company.

References

1. O'Rourke, M. F., A. Pauca, and X. J. Jiang. Pulse wave analysis. *Br. J. Clin. Pharmacol.* 51:507–522, 2001.
2. Desbiens, L.-C., C. Fortier, A.-C. Nadeau-Fredette, F. Madore, B. Hametner, S. Wassertheurer, M. Agharazii, and R. Goupil. Prediction of cardiovascular events by pulse waveform parameters: analysis of CARTaGENE. *J. Am. Heart Assoc.*11:e026603, 2022.
3. Salvi, P., A. Grillo, and G. Parati. Noninvasive estimation of central blood pressure and analysis of pulse waves by applanation tonometry. *Hypertens. Res.* 38:646–648, 2015.
4. Drzewiecki, G. M., J. Melbin, and A. Noordergraaf. Arterial tonometry: review and analysis. *J. Biomech.* 16:141–152, 1983.
5. Liang, F. Numerical validation of a suprasystolic brachial cuff-based method for estimating aortic pressure. *Biomed. Mater. Eng.* 24:1053–1062, 2014.
6. Costello, B. T., M. G. Schultz, J. A. Black, and J. E. Sharman. Evaluation of a brachial cuff and suprasystolic waveform algorithm method to noninvasively derive central blood pressure. *Am. J. Hypertens.* 28:480–486, 2015.
7. Hwang, M. H., J. K. Yoo, H. K. Kim, C. L. Hwang, K. Mackay, O. Hemstreet, W. W. Nichols, and D. D. Christou. Validity and reliability of aortic pulse wave velocity and augmentation index determined by the new cuff-based SphygmoCor Xcel. *J. Hum. Hypertens.* 28:475–481, 2014.
8. Horváth, I. G., Á. Németh, Z. Lenkey, N. Alessandri, F. Tufano, P. Kis, B. Gaszner, and A. Cziráki. Invasive validation of a new oscillometric device (Arteriograph) for measuring augmentation index, central blood pressure and aortic pulse wave velocity. *J. Hypertens.* 28:2068, 2010.
9. Pucci, G., J. Cheriyan, A. Hubsch, S. S. Hickson, P. R. Gajendragadkar, T. Watson, M. O'Sullivan, J. Woodcock-Smith, G. Schillaci, I. B. Wilkinson, and C. M. McEniery. Evaluation of the Vicorder, a novel cuff-based device for the noninvasive estimation of central blood pressure. *J. Hypertens.* 31:77–85, 2013.
10. Weber, T., S. Wassertheurer, M. Rammer, E. Maurer, B. Hametner, C. C. Mayer, J. Kropf, and B. Eber. Validation of a brachial cuff-based method for estimating central systolic blood pressure. *Hypertension*. 58:825–832, 2011.
11. Miyashita, H. Clinical assessment of central blood pressure. *Curr. Hypertens. Rev.* 8:80–90, 2012.
12. Wassertheurer, S., J. Kropf, T. Weber, M. van der Giet, J. Baulmann, M. Ammer, B. Hametner, C. C. Mayer, B. Eber, and D. Magometschnigg. A new oscillometric method for pulse wave analysis: comparison with a common tonometric method. *J. Hum. Hypertens.* 24:498–504, 2010.
13. Babbs, C. F. Oscillometric measurement of systolic and diastolic blood pressures validated in a physiologic mathematical model. *Biomed. Eng. Online*. 11:56, 2012.
14. Fabian, V., L. Matera, K. Bayerova, J. Havlik, V. Kremen, J. Pudil, P. Sajgalik, and D. Zemanek. Noninvasive assessment of aortic pulse wave velocity by the brachial occlusion-cuff technique: comparative study. *Sensors*. 19:3467, 2019.
15. Schlichting, H., and K. Gersten. Boundary-Layer Theory. New York: Springer, p. 805, 2016.
16. Holman, J. P. Heat Transfer—Si Units—Sie. New Delhi: McGraw-Hill Education (India) Pvt Limited, p. 674, 2002.
17. Womersley, J. R. Method for the calculation of velocity, rate of flow and viscous drag in arteries when the pressure gradient is known. *J. Physiol.* 127:553–563, 1955.
18. Zamir, M. Pulsatile flow in an elastic tube. *Phys. Pulsatile Flow*. 2000. https://doi.org/10.1007/978-1-4612-1282-9_5.
19. Nield, D. A., and A. V. Kuznetsov. Forced convection with laminar pulsating flow in a channel or tube. *Int. J. Therm. Sci.* 46:551–560, 2007.
20. San, O., and A. E. Staples. An improved model for reduced-order physiological fluid flows. *J. Mech. Med. Biol.* 12:1250052, 2012.
21. Love, A. E. H. A Treatise on the Mathematical Theory of Elasticity. Charleston: BiblioLife, 2010.
22. Whirlow, D. K., and W. T. Rouleau. Periodic flow of a viscous liquid in a thick-walled elastic tube. *Bull. Math. Biophys.* 27:355–370, 1965.
23. Taylor, L. A., and J. H. Gerrard. Pressure-radius relationships for elastic tubes and their application to arteries. Part 1—theoretical relationships. *Med. Biol. Eng. Comput.* 15:11–17, 1977.
24. Trube, A. S. Compressibility of natural gases. *J. Pet. Technol.* 9:69–71, 1957.
25. Natarajan, K., H.-M. Cheng, J. Liu, M. Gao, S.-H. Sung, C.-H. Chen, J.-O. Hahn, and R. Mukkamala. Central blood pressure monitoring via a standard automatic arm cuff. *Sci. Rep.* 7:14441, 2017.
26. Agnoletti, D., Y. Zhang, P. Salvi, C. Borghi, J. Topouchian, M. E. Safar, and J. Blacher. Pulse pressure amplification, pressure waveform calibration and clinical applications. *Atherosclerosis*. 224:108–112, 2012.
27. Magder, S. Clinical usefulness of respiratory variations in arterial pressure. *Am. J. Respir. Crit. Care Med.* 169:151–155, 2004.
28. McVeigh, G. E., C. W. Bratteli, D. J. Morgan, C. M. Alinder, S. P. Glasser, S. M. Finkelstein, and J. N. Cohn. Age-related abnormalities in arterial compliance identified by pressure pulse contour analysis. *Hypertension*. 6:1392–1398, 1999.